A modeling study on the revere cycle defrosting of an air source heat pump with the melted frost downwards flowing away and local drainage

A modeling study on the revere cycle defrosting of an air source heat q pump with the melted frost downwards flowing away and local drainage

Mengjie Song[a,b,c], Gongnan Xie[d], Libor Pekař[e], Ning Mao[f,*], Minglu Qu[b]

[a]*Department of Energy and Power Engineering, School of Mechanical Engineering, Beijing Institute of Technology, Beijing, China*

[b]*School of Environment & Architecture, University of Shanghai for Science & Technology, No.516, Jungong Road, Shanghai, China*

[c]*CAS Key Laboratory of Cryogenics, TIPC, China*

[d]*Department of Mechanical and Power Engineering, School of Marine Science and Technology, Northwestern Polytechnical University, Xi'an 710072, Shaanxi, China*

[e]*Department of Automation and Control Engineering, Faculty of Applied Informatics, Tomas Bata University in Zlín, Nad Stráněmi 4511, 76005 Zlín, Czech Republic*

[f]*Department of Gas Engineering, College of Pipeline and Civil Engineering, China University of Petroleum (East China), Qingdao, China*

[*]*Corresponding author. E-mail address: maoningcas@hotmail.cm (N. Mao).*

ABSTRACT

Reverse cycle defrosting is widely used for air source heat pumps. When a multi-circuit heat exchanger is vertically installed in a heat pump as an outdoor coil, the melted frost could be kept downwards flowing or locally drained during defrosting by using water collecting trays. To analyze the performance differences of melted frost, two defrosting models were developed and previously reported by authors. In this study, the defrosting performance of an air source heat pump was numerically investigated based on the two models, with the melted frost downwards flowing away or local drainage considered. The following physical parameters are predicted and analyzed, including the thermal resistance of refrigerant, temperature of melted frost on tube and fin's surface, mass of melted frost and energy consumption from refrigerant during defrosting. As calculated, after the melted frost locally drained, the predicted total energy consumption could be decreased from 898.1 kJ to 727.5 kJ, and defrosting efficiency increased from 47.5% to 57.6%. This work is helpful to optimizing the intelligent control strategy of an air source heat pump unit, as well as saving energy for buildings.

Keywords: Air source heat pump, reverse cycle defrosting, multi-circuit outdoor coil, modeling study, melted frost

1. Introduction

Air source heat pump (ASHP) units are widely used for hot water supply and room heating in recent decades [**1**]. Governmental subsidy policies also promote their development due to the environmental friendly performance of ASHP and the server air pollution in heating season of Northern China or

Ulaanbaatar [**2,3**]. When frost accumulated on the surface of outdoor coil in an ASHP unit, defrosting becomes necessary. There are two types of defrosting methods, mechanical defrosting and thermal defrosting [**4**]. Mechanical defrosting needs more components for an ASHP unit, which also affects the durability of outdoor coil and increases the initial cost. Thus, thermal defrosting methods are widely considered, including compressor shut down defrosting, hot water spray defrosting, electric heating defrosting, hot gas bypass defrosting, and reverse cycle defrosting. Reverse cycle defrosting is changing the roles of indoor coil and outdoor coil during defrosting by using a four-way valve, and thus the condenser and evaporator changed [**5**]. The indoor air thermal energy will be taken and used for defrosting, which is previously transferred from the ambient air in frosting/heating mode at a higher coefficient of performance (COP). Thus, the defrosting duration becomes short, and economic performance much better. Reverse cycle defrosting becomes the most widely used method.

To improve the performance of reverse cycle defrosting, series of work were carried out [**6**]. For example, an experiment investigation of reverse cycle defrosting methods on an ASHP unit with thermal expansive valve as the throttle regulator was carried out by Ding et al. [**7**]. By using a solenoid valve by-pass the thermal expansive valve used in the defrosting mode, the defrosting duration could be efficiently shorted, and the system could resume heating mode smoothly after the defrosting process. The insufficient of heat supply problem during reverse cycle defrosting was also found by Hu et al. [**8**], and a phase change material thermal storage unit was used in the ASHP unit. The experimental results suggested that (1) the defrosting time was shorted by ∼3 min or 38%, (2) the risk of shutting down the ASHP unit due to low suction pressure was minimized, and (3) the mean indoor coil surface temperature during defrosting was improved about 25 K. This method was also used in a cascade ASHP unit by Qu et al. [**9,10**], multi-split ASHP unit by Dong et al. [**11,12**], air-cooled household refrigerators by Liu et al. [**13,14**], respectively. By increasing the evenness of frost accumulation on the surface of a multi-circuit outdoor coil at the start of a defrosting operation, the efficiency of reverse cycle defrosting was improved by Song et al. [**15,16**]. To avoid mal-defrosting phenomenon mentioned by Wang et al. [**17**], defrosting control strategies were also widely investigated [**18,19**]. The time-based start defrosting [**20**] and temperature-based end defrosting control strategies are experimentally investigated by Song et al. [**21,22**]. For the reported ASHP unit, the most suitable pre-set time and temperature for reverse cycle defrosting is at around 55 min and 18.5 °C, respectively.

However, because defrosting is a complex process involving spatial and time variations as well as many other indeterminate factors resulted from transient cycling which may last for only a few minutes, limited models about defrosting were developed and reported. Typically, a validated defrosting model for an ASHP unit using capillary tube was developed by Liu et al. [**23**], where distributed modeling was used for both evaporator and condenser because of their importance during reverse cycle defrosting. An electric defrosting model for a finned-tube outdoor coil was reported by Alebrahim and Sherif [**24**] in 2002, which using the enthalpy method to predict defrosting duration and frost surface temperature profiles. A modelling study on the heat storage and release process of phase change material thermal storage unit in an ASHP unit during frosting and defrosting was carried out by Hu et al. [**25**]. The deviation conditions were demonstrated acceptable with the mean average temperature differences at the small range of -0.71 ∼ 1.64 °C. A modeling of transient characteristics of an ASHP unit with vapor injection during reverse cycle defrosting was reported by Qiao et al.[**26**]. Component submodels for the multi-circuit heat exchangers, vapor injection scroll compressor, flash tank, check valve, and pipes, etc. were all considered. But the model was not validated with corresponding experimental results. The defrosting efficiency was finally predicted at 17.7%, which meets the result reported by Niederer [**27**], at a range of 15-25%. However, most reported models are based on the whole ASHP unit during defrosting, and many sections or components are included. Thus many assumptions, empirical formula

and parameters are used, leading to low precision defrosting models. Even in some studies the final results seem reasonable [**26**], the small deviation maybe result from error superposition.

To investigate the heat transfer and flow mechanism during reverse cycle defrosting, the multi-circuit outdoor coil attracts more and more attentions. A semi-empirical model for the defrosting on the airside of a four-circuit outdoor coil in an ASHP unit was developed by Qu et al. [**28**]. Different from aforementioned defrosting modeling studies, the negative effects of melted frost on defrosting performance were considered and quantitatively studied [**29**]. Later, the effects of the melted frost on defrosting performance were experimentally investigated by Song et al. [**30,31,32**]. In consideration of the energy used to heat the metal in an outdoor coil accounted for as much as 16.5% of the total defrosting energy use during defrosting [**28,33**], two new models for with one and three water collecting trays installed between circuits were further developed by Song et al. [**34**]. Water collecting trays make two conditions for the melted frost, downwards flowing always and local drainage, as shown in **Fig. 1**(a) and (b), respectively. It is also the first defrosting model, in which the status of frost distribution was considered. Based on the two validated models, a modeling study on varying heat (via refrigerant) supply to each refrigerant circuit in a three-circuit outdoor coil to alleviate uneven defrosting was reported [**35**]. As demonstrated, defrosting duration was predicted a reduction of 7 s by fully closing the modulating valve on the top circuit when its defrosting terminated.

Moreover, after the defrosting models validated with experimental results, some parameters which are hardly possible to be measured could be predicted, including the temperature of melted frost, frost melting rate, thermal resistance of refrigerant during defrosting etc. These fundamental data are not only meaningful to understand the heat transfer and flow mechanism during defrosting, but also make contributions to the energy saving and system optimization. However, in open literatures, scare of these parameters were calculated and reported. Therefore, basing on previously developed and validated models, the effects of melted frost on system defrosting performance were predicted. At the same time, many defrosting parameters were numerical investigated and reported in this paper. Firstly, the model used and its validation were shortly described. This is followed by presenting these numerical results. After the result analysis and discussions on the defrosting models given, the conclusions are finally listed. This study is expected to be a benefit for system optimization of ASHP units and energy saving for buildings.

2. Description of defrosting models

2.1. The models and assumptions

The defrosting models used in this work were previously reported in Ref. [**34**]. Here, they will be shortly introduced. The two models were built for a three-circuit outdoor coil in an experimental ASHP unit, which are semi-empirical models. For a traditional ASHP unit, the melted frost is always downwards flowing away along the surface of vertical outdoor coil during defrosting, as shown in **Fig. 1**(a). To analyze the effects of melted frost on system defrosting performance, a new three-circuit outdoor coil was made with three water collecting trays installed under each circuit. During defrosting, the melted frost could be locally drained in this novel ASHP unit, as shown in **Fig. 1**(b).

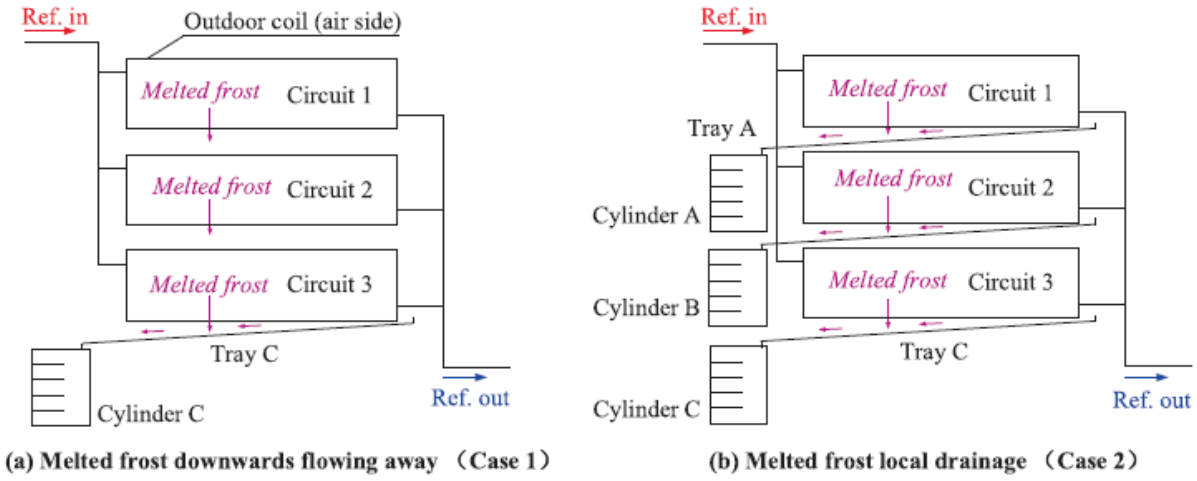

Fig. 1. Illustration of melted frost downwards flowing away and local drainage.

Before reverse cycle defrosting mode is operated, the frosting evenness value was fixed higher than 90%. In the experiment, the opening degrees of each valve located at each circuit were fixed. The two conditions, with melted frost downwards flowing away and local drainage, were achieved by keeping or taking away the water collecting trays, respectively. In this study, they are named as Case 1 and Case 2 for simplicity and marked in **Fig. 1**.

To build the two defrosting models, the assumptions are important, and thus all of them were listed here. Meanwhile, the four defrosting stages divided by physical process were shown in **Fig. 1**, as well as the mass and energy flows.

1) The convective heat transfer between frost and ambient air in the first two stages was neglected.

2) The thermal conductivities of tubes and fins were much higher than those of frost and retained water.

3) The mass flow rate of refrigerant was evenly distributed into the three refrigerant circuits during defrosting, and the frost was assumed to be uniformly accumulated over the coil surface before starting defrosting.

4) The movement of the melted frost layer was considered to be a flowing boundary.

5) During the third stage, the retained water in each control volume was in a dynamic equilibrium, i.e., the difference between the mass of water entering into a control volume and that flowing away from the control volume was equal to the rate of frost melting within the control volume.

6) During defrosting, the melted frost infiltrated into the porous structure of frost. The contact area between frost and the melted frost would increase as water flowed downwards, suggesting that the flow resistance was increased downwards along the surface of outdoor coil.

7) During defrosting, there was no frost chip or debris flowing into a down circuit or a water collecting tray(s).

8) During defrosting, the melted frost left on trays or vaporized from trays and cylinders was neglected.

9) In the process of the melted frost falling into a down circuit or a water collecting tray, the heat dissipated from the melted frost to ambient air was negligible because the falling distance was small.

10) The total mass of the frost was experimentally obtained at 1,050 g, thus following Assumption (iii), the mass of frost formed on the surface of each circuit was 350 g [**30**].

11) At 40 s into defrosting, the preheating stage (first stage) was over.

12) At 90 s into defrosting, the frost melting without water flowing away from a circuit stage was over.

2.2. Equations used at four defrosting stages

When developing the two mathematical models, the entire air-side of the outdoor coil surface was divided into three control volumes (CV), corresponding to the three circuits shown in **Fig. 1**. For each CV, lumped parameter modeling approach was applied. To analyze the flow of the melted frost into, or away from a CV during defrosting, a defrosting process was divided into four stages, (1) preheating, (2) frost melting without water flowing away from a circuit, (3) frost melting with water flowing away from a circuit, and (4) water layer vaporizing. It is also according to the time sequence of physical occurrence process [**28,34**]. **Fig. 2** shows the mass and energy flows at four stages during defrosting.

The two models were developed by applying the energy and mass conservation in each of the three CVs, at each of the fourth defrosting stages. The equations used at each stage in Case 1 were listed in Table 1. As seen, only in the Stage 3, the equations are different between CV1 and other two CVs. This is because the mass transfer, melted frost downwards flowing, occurs at this stage. For Case 2, the energy and mass balance equations at Stages 1, 2 ad 4 are same to those in Case 1. At Stage 3, only the energy and mass balance equations for CV1 are used for three CVs. All the nomenclatures could be found in Ref. [**34**]. In addition, the submodels of water collecting trays in two cases are same, which could also be found in Ref. [**34**].

2.3. Input parameters and model validation

The following experimental parameters measured during defrosting were used as the inputs to the models, including refrigerant flow rate, tube surface temperatures at inlets of each circuit, temperature of ambient air surrounding the outdoor coil, and compressor discharge pressure, etc. In **Figs. 3 and 4**, the measured flow rate and calculated enthalpy value of input refrigerant in two cases are presented, respectively. As seen in **Fig. 3**, the curve of mass flow rate of refrigerant clearly shows us three stages. From 0 s to 70 s into defrosting, it fluctuated a lot as increasing. It should contain the preheating stage and part of frost melting without water flowing away from a circuit stage. Then, it changed to steeply increase from 70 s to 160 s. The melted frost taking a lot of energy from refrigerant, and thus the flow rate also increased quickly. When it reached 160 s into defrosting, the rate of energy consumption would decreased due to melted frost flowing away. The refrigerant mass flow rate decreased suddenly and kept at a steady value. All the status of refrigerant mass flow rate result from the heat and mass transfer status during physical defrosting, but also reflected in the defrosting parameters in this model as the input values.

In the two defrosting models, the calculated enthalpy values of input refrigerant in two cases were also inputs. Different from that shown in **Fig. 3**, the data in **Fig. 4** is always increasing from 0 s to about 160 s into defrosting. This is because the energy from refrigerant was always consumed during defrosting at this period. As the start stage, the heat transfer between fin and frost is low, and increases a lot when frost melted into water, just like from Stage 1 to Stage 2 shown in **Fig. 2**. When the melted frost flows downwards along the surface of outdoor coil, the heat transfer still increases due to evaporation existing for residual water. It comes to Stage 4 from Stage 3, as shown in **Fig. 2**. After 160 s into defrosting, the curve seems steady, and the heat transfer status is nearly unchanged. At this stage, the heat transfer is between high temperature tube and fin and the low temperature ambient air. And the reverse cycle defrosting process is nearly terminated. As seen in **Fig. 4**, the curves of Case 2 have the similar trends to those of Case 1, but the later ones are a little higher. This reflects the negative effects of melted frost on defrosting. That means, after the melted frost locally drained, the enthalpy value of input refrigerant could be decreased, and some energy saved during defrosting.

The two models were finally validated by comparing four predicted key operating parameters, defrosting duration; tube surface temperatures at exit of each circuit; temperature variations of the melted frost collected in three water collecting cylinders and the mass of the melted frost collected in each cylinder. Here, the validation of tube surface temperatures at exits of the three circuits in Cases 1 and 2 are shown in **Figs. 5 and 6**, respectively. As seen in **Fig. 5**, the predicted defrosting durations for each circuit reaching 24 °C are at 173 s, 179 s, and 186 s for Circuits 1-3, respectively.

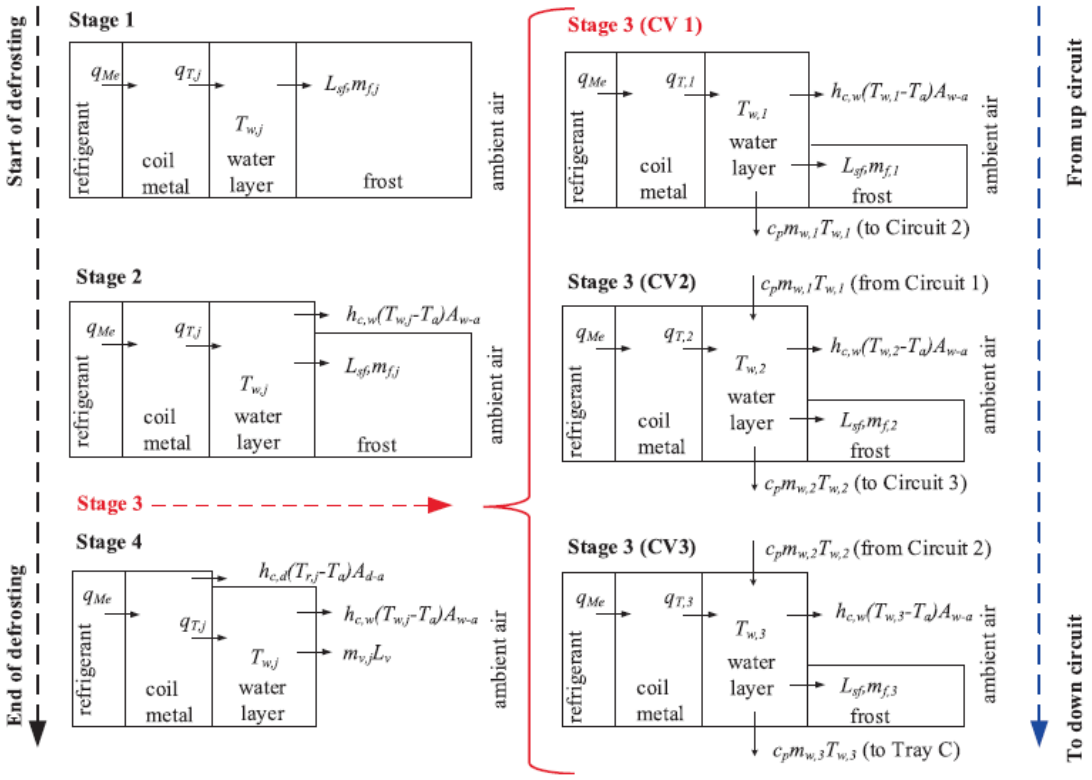

Fig. 2. Schematics of mass and energy flows at four stages during defrosting.

Table 1 Energy and mass balance equations in the four stages in Case 1.

Table 1
Energy and mass balance equations in the four stages in Case 1.

Stage	Energy and mass balance equations
1	$q_j = L_{sf} m_{f,j} + c_p \frac{d(M_{w,j} T_{w,j})}{dt} + q_{Me};\ M_{w,j} = \int_0^t m_{f,j} dt (j = 1-3)$
2	$q_j = L_{sf} m_{f,j} + c_p \frac{d(M_{w,j} T_{w,j})}{dt} + h_{c,w}(T_{w,j} - T_a) A_{f-a} + q_{Me};\ M_{w,j} = \int_0^t m_{f,j} dt (j = 1-3)$
3	For CV1 (Circuit 1): $q_1 = L_{sf} m_{f,1} + c_p M_{w,\max} \frac{dT_{w,1}}{dt} + c_p m_{w,1} T_{w,1} + h_{c,w}(T_{w,1} - T_a) A_{f-a} + q_{Me};\ m_{w,1} = m_{f,1}$ For other two CVs (Circuits 2 and 3): $q_j + c_p m_{w,j-1} T_{w,j-1} = L_{sf} m_{f,j} + c_p M_{w,\max} \frac{dT_{w,j}}{dt} + c_p m_{w,j} T_{w,j} + h_{c,w}(T_{w,j} - T_a) A_{f-a} + q_{Me} m_{w,j} = m_{f,j} + m_{w,j-1}\ (j = 2, 3)$
4	$q_j = c_p \frac{d(M_{w,j} T_{w,j})}{dt} + h_{c,w}(T_{w,j} - T_a) A_{w-a} + h_{c,d}(T_{r,j} - T_a) A_{d-a} + m_{v,j} L_v + q_{Me};\ M_{w,j} = M_{w,\max} - \int_0^t m_{v,j} dt\ (j = 1-3)$

While the three durations in experiments are 173 s, 182 s, and 185 s. The deviations of tube surface temperature are very small, and could be accepted. From 115 s to 150 s into defrosting, the deviations for three circuits seems much larger than other time. The experimental data is much higher than predicted data for Circuits 1 and 2, and smaller for Circuit 3. The deviation ranges for Circuits 1 and 2 are also smaller than that of Case 3. This makes the total deviations, positive and negative deviations, becomes much smaller. In fact, at this period, as the downwards flowing of melted frost, the even distribution of refrigerant is affected a lot. The temperature deviations result from the coupled effects of melted frost flowing and uneven refrigerant distribution.

In **Fig. 6**, the predicted defrosting durations for each circuit reaching 24 °C are all at 169 s for three circuits, while the experimental results are 169 s, 167 s and 170 s for Circuits 1-3, respectively. Clearly, the deviations for tube surface temperature are much smaller than that shown in **Fig. 5** in Case 1. Similar to that shown in **Fig. 5**, from 90 s to 140 s into defrosting, there are also positive and negative deviations for Circuits 1 and 2, respectively. The positive deviation means the predicted value is larger than the experimental result, and negative deviation in versa. In Case 2, this period seems about 10 s earlier than that in Case 1. This results from the defrosting duration decreased due to the melted frost locally drained. Compared with that shown in Fig. 5, the smaller deviation range in **Fig. 6** also results from the coupled effects of melted frost flowing and uneven refrigerant distribution. But in Case 2, the influence from melted frost was effectively decreased.

Finally, in Case 1, compared with the measured data, the maximum deviations of predicted results for Circuits 1-3 were -1.8 °C, —1.2 °C, and 2.4 °C, respectively. The average deviations between measured and predicted results for Circuits 1-3 were —0.2 °C, 0 °C and 0.4 °C, respectively. In Case 2, the maximum and average deviations of predicted results for three circuits were calculated at 2.5 °C, —1.8 °C, —1.2 °C, and 0.7 °C, —0.6 °C, —0.1 °C, respectively. Therefore, it was considered that the two semi-empirical models were experimentally validated, and the validated models could be further used to quantitatively analyze the defrosting performances of an ASHP unit. When developing the two models, the influence from thermal resistance of refrigerant is big. Additionally, it is meaningful to analyze the fluctuation of thermal resistance of refrigerant during defrosting due to the complicated heat transfer process, which is coupled with mass transfer and flow of melted frost. In a recent frosting study, this parameter was also calculated as thermal resistance of evaporator by using empirical formulas by Shen etc. [**36**]. Therefore, in this study, the experimental tube surface temperatures at the outlet of each circuits in two cases were used as inputs. The accuracies of the two models could also be improved due to the influence of thermal resistance of refrigerant avoided.

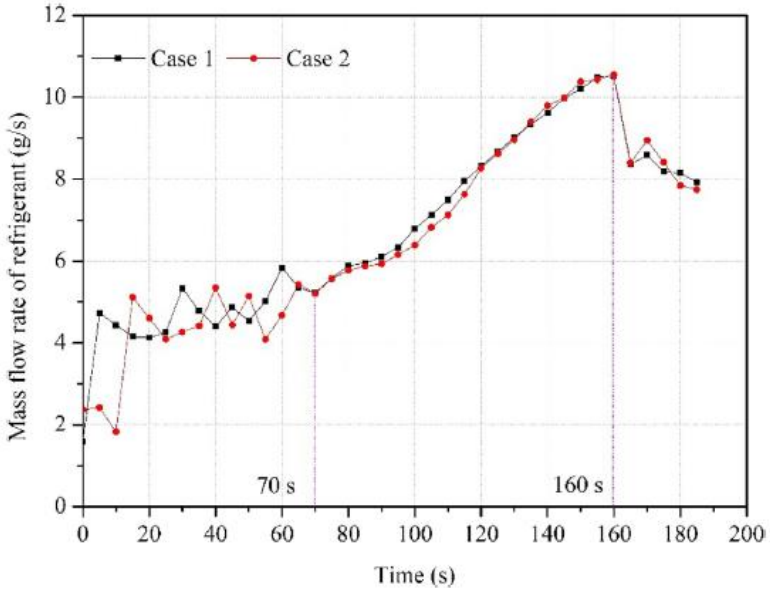

Fig. 3. Refrigerant mass flow rate at the inlet of each circuit in two cases.

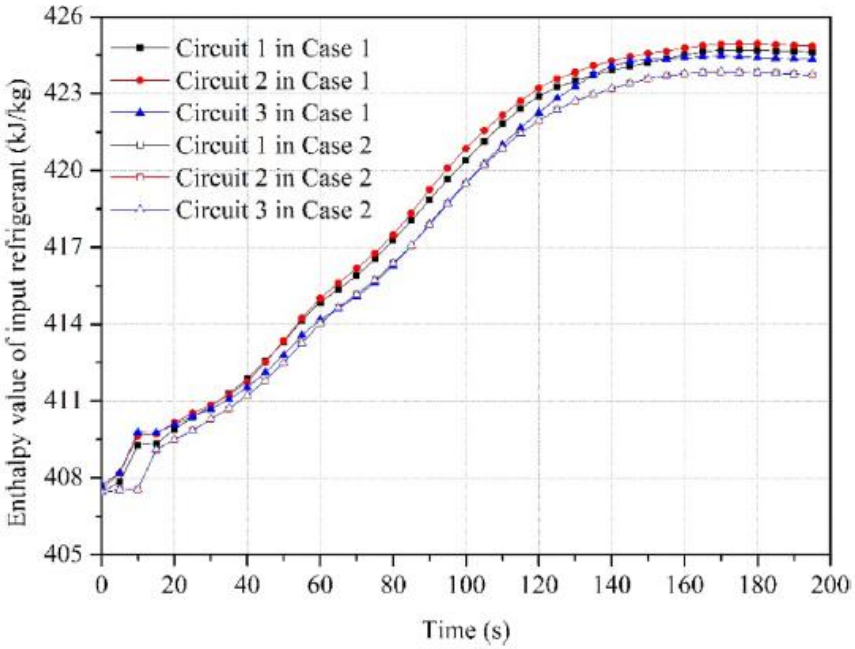

Fig. 4. Enthalpy value of input refrigerant in two cases.

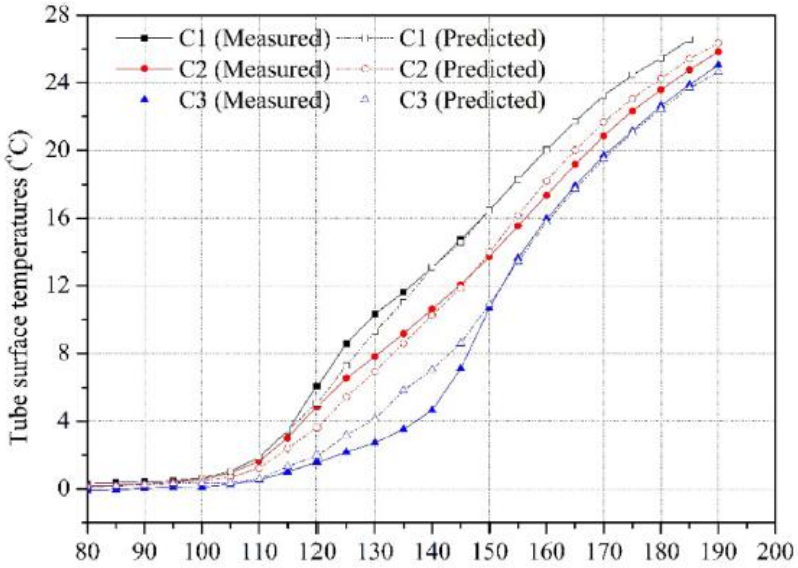

Fig. 5. Validation of tube surface temperatures at exits of the three circuits in Case 1.

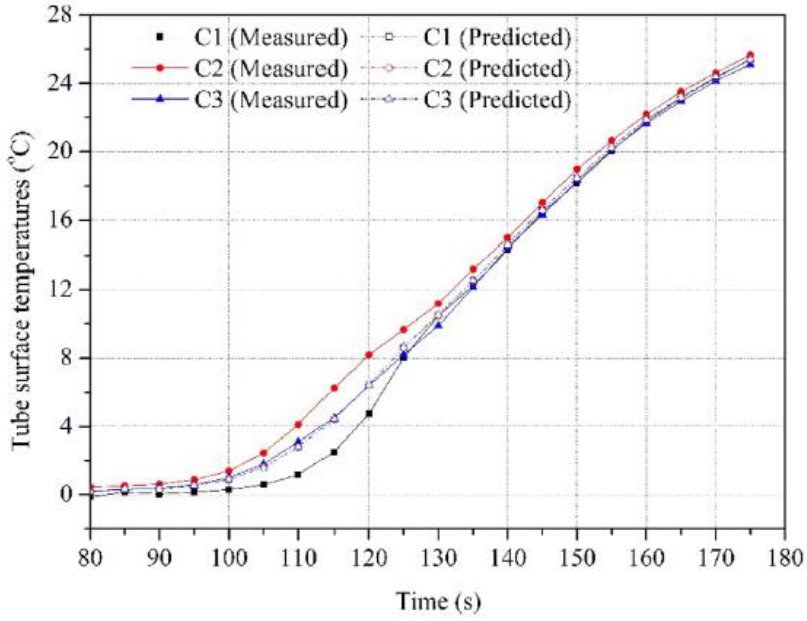

Fig. 6. Validation of tube surface temperatures at exits of the three circuits in Case 2.

3. Results of modeling study

Based on two validated models, some of predicted results were reported here, as shown in **Figs. 7-15**. The input values were from 0 s to 200 s into defrosting, and thus the horizontal axis for **Figs. 7-14** were also at this period. Because the effect of melted frost is the key research object, in **Figs. 7 and 8**, temperature of melted water on each circuit's surface in Cases 1 and 2 are firstly presented, respectively.

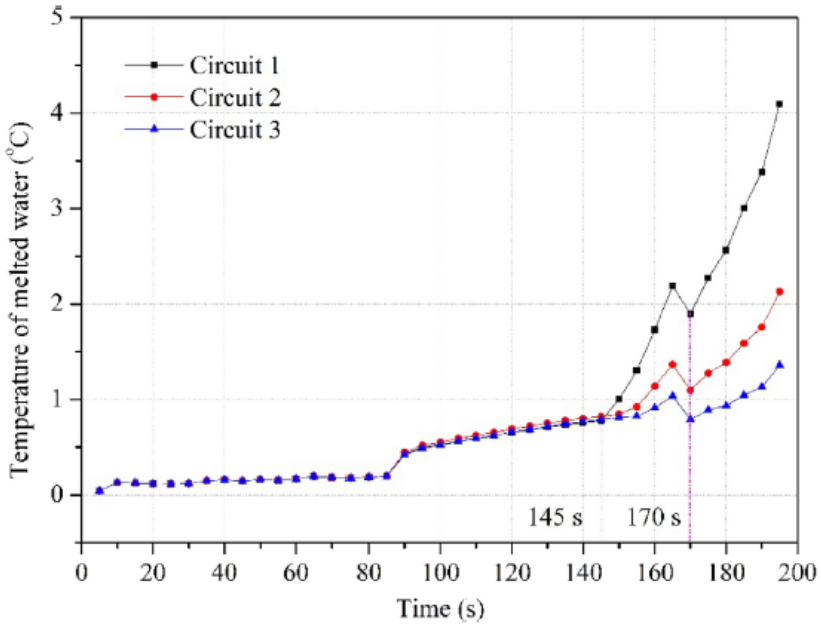

Fig. 7. Temperature of melted water on each circuit's surface in Case 1.

Secondly, the predicted mass of melted frost during defrosting in two cases are shown in **Figs. 9 and 10**. Thirdly, the fluctuations of thermal resistance of refrigerant during defrosting in two cases are meaningful in this study, and thus they are shown in **Figs. 11 and 12**. Fourthly, to quantitatively analyze the effect of melted frost downwards flowing away and locally drained, energy used from the refrigerant were calculated at each 5 s in two cases, and presented in **Figs. 13 and 14**. Finally, the calculated data of total energy consumed during defrosting are shown in **Fig. 15**.

The predicted temperature of melted water on the surface of each circuit during defrosting is shown in **Fig. 7**, with the melted frost freely downwards flowing away from the up circuit(s) and into the down circuit(s). This parameter is very difficult or even impossible to be measured at experiment due to the dynamic heat and mass transfer. Meanwhile, it is important to develop the model as an intermediate variable. This is the reason why we choose to investigate it with this model. As seen, it kept at nearly 0 °C from 0 s to 85 s, which is at the first stage, preheating stage. The water layer or film between frost and tube surface was formed, and thus the water temperature is always the temperature of mixture of frost and water. When it comes to 85 s to 145 s, the temperature increased slowly, due to the thickness of water layer increasing as the frost melting. As the frost layer decreased, the water layer was heated. From 145 s to the end of defrosting, the melted water was heated, and thus its temperature increased always. At the end of simulation, it reached nearly 7 °C for Circuit 1. At the same time, it is easy to find that the temperature at three circuits are different. As the melted frost downwards flowing, the water temperature of Circuit 1 is the highest, and that of Circuit 3 the lowest.

This reflects the negative effects of melted frost during defrosting. At 170 s, there is a suddenly decrease. This is also the start of quickly increasing for the three curves. At this time point, the main heat transfer role changed from heating the melted frost to vaporizing it. **Fig. 8** shows the predicted temperature of melted water on the surface of each circuit during defrosting in Case 2, with the melted frost locally drained. Similar trends to those shown in **Fig. 7**, the temperature of melted frost for three circuits are always the same. After 140 s into defrosting, the temperature becomes higher than that in Circuit 1 in Case 1. This also reflects that, after the melted frost locally drained during defrosting, the temperature of tube and fin surface is also increased.

Figs. 9 and 10 show the mass of melted frost during defrosting in Cases 1 and 2, respectively. This parameter is also impossible to be measured in experiments. Therefore, in many frosting and defrosting studies, the average frosting or defrosting rates are used [**36,37,38**]. As shown in **Fig. 9**, after 140 s, 145 s and 150 s into defrosting, the mass of melted frost become 0 g for Circuits 1-3, respectively. Before the termination of frost melting and flowing stages, the figure shows us two clear periods. The first period is from 0 s to 80 s, when the masses of melted frost are always the same for three circuits due to no melted frost flowing away from the circuit. The second period is from 80 s to about 145 s, when the mass of melted frost in Circuit 1 is always the highest and in Circuit 3 lowest due to the melted frost downwards flowing away from up circuit(s) to down circuit(s). The melted frost from up cir-cuit(s) delay the frost melting rate of the frost on the surface of down circuit(s). Although there would be more water on the surface of down circuit(s), here the curve shows us the frost formed on the surface of this circuit melted. Because the melting durations for down circuits, Circuits 2 and 3 in this study, are prolonged, and thus the peak values for them are a little lower. As seen, the three peak values for Circuits 1-3 are 4.30 g, 3.99 g and 3.61 g, respectively. This also reflects the negative effects of melted frost downwards flowing during defrosting. In Fig. 10, the masses of melted frost for three circuits are always the same due to the melted frost locally drained, and their predicted data are similar to that in Circuit 1 shown in **Fig. 9**.

Figs. 11 and 12 show the fluctuation of predicted thermal resistance of refrigerant during defrosting in Cases 1 and 2, respectively. Similar to the previous two predicted parameters, temperature and mass of melted frost, the thermal resistance of refrigerant also shows us clear periodic law. The curves are divided into 5 periods, which are clearly influenced by the stage division of defrosting process as shown in **Fig. 2**. In **Fig. 11**, the thermal resistance increases steadily from 0 s to 80 s into defrosting, at the Period 1. Because no melted frost downwards flowing, and thus the values of three circuits are the same, until after this period. At Period 2, from 80 s to 140 s into defrosting, the heat transfer is influenced by the flowing of melted frost. Because there is no melted frost flowing into Circuit 1, and more into Circuit 3 than Circuit 2, the curves show the highest thermal resistance for Circuit 1 and lowest for Circuit 3. Their values keep steady at this period, and then suddenly increase at Periods 3 and 4, about 20 s and 26 s, respectively. At the 160 s, into defrosting, the curves show us a decrease due to the change of the main heat transfer from heating the melted frost to vaporization. When it comes to the Period 5, it starts slowly decreasing due to few residual water left. The heating mode is changing to heating the ambient air after 185 s into defrosting.

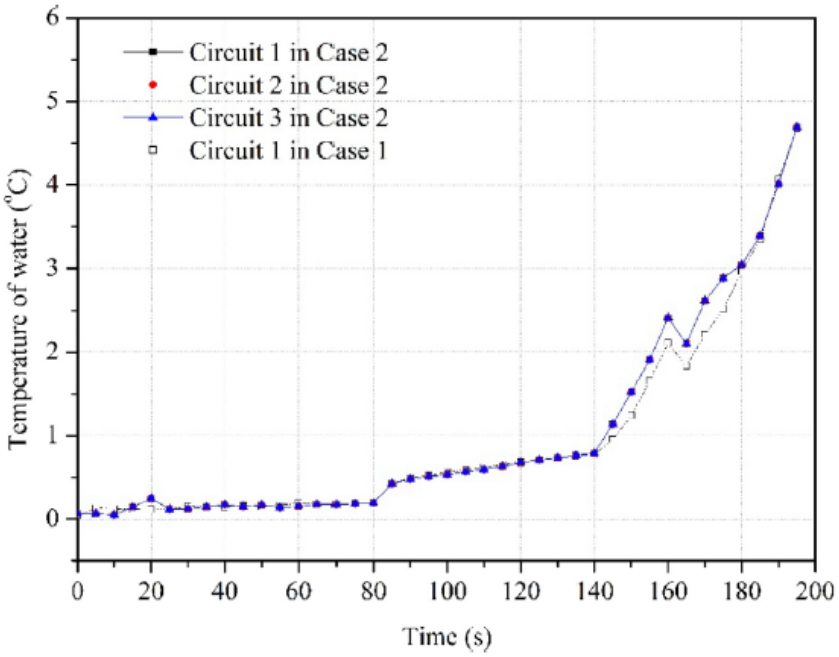

Fig. 8. Temperature of melted water on each circuit's surface in Case 2.

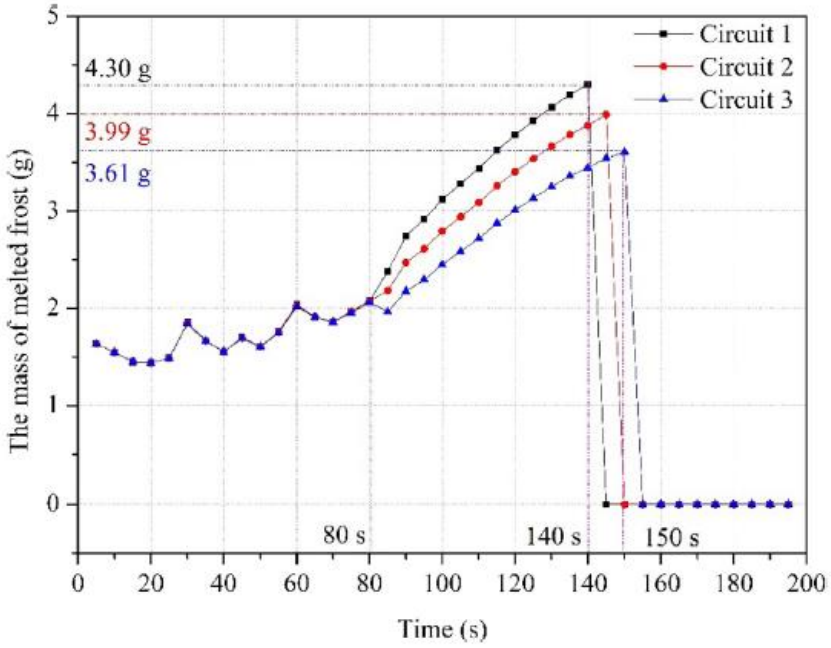

Fig. 9. The mass of melted frost during defrosting in Case 1.

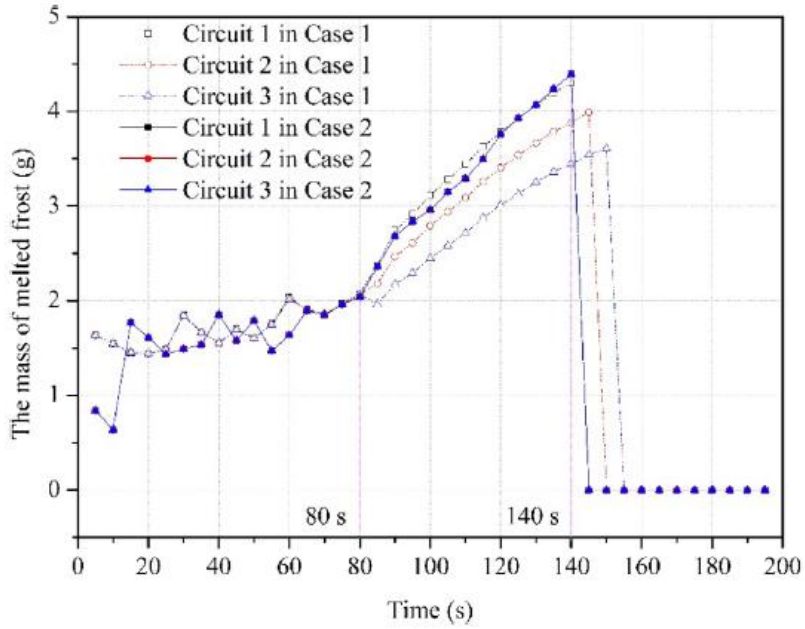

Fig. 10. The mass of melted frost during defrosting in Case 2.

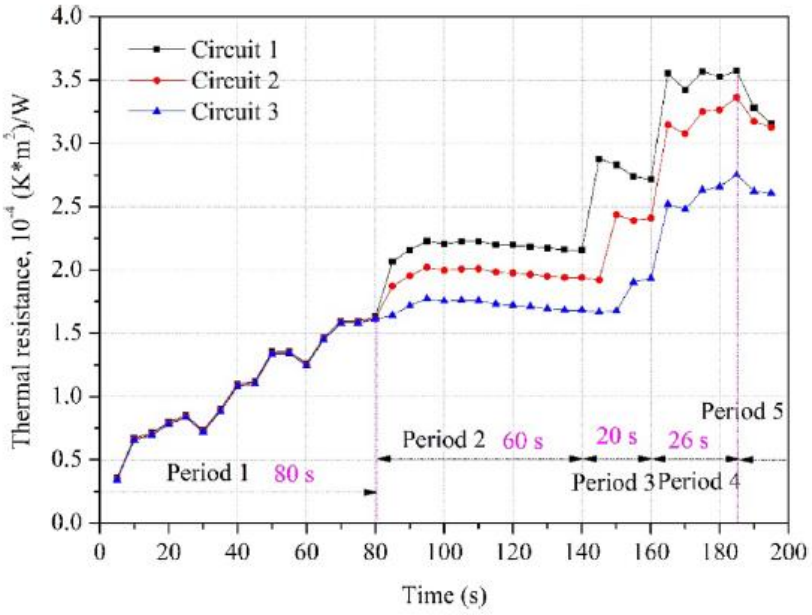

Fig. 11. Thermal resistance of refrigerant during defrosting in Case 1.

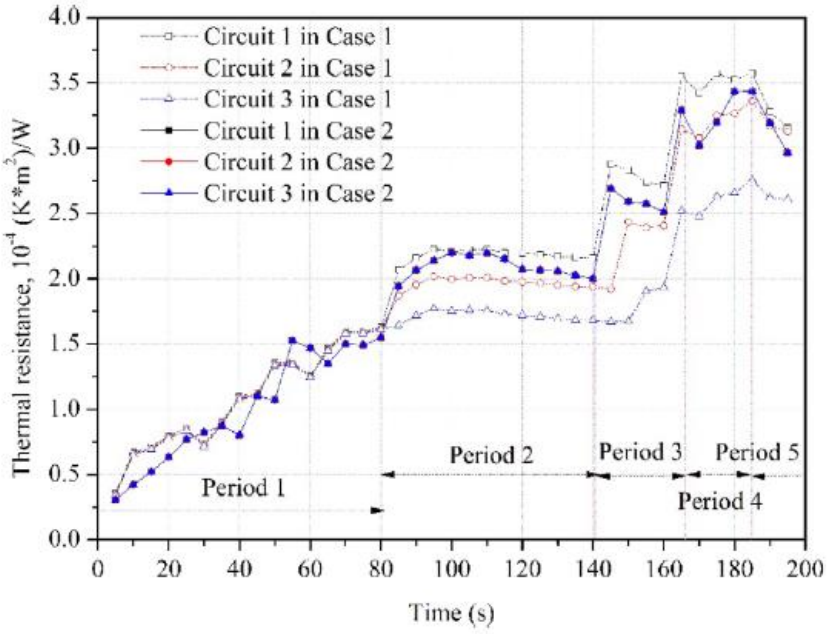

Fig. 12. Thermal resistance of refrigerant during defrosting in Case 2.

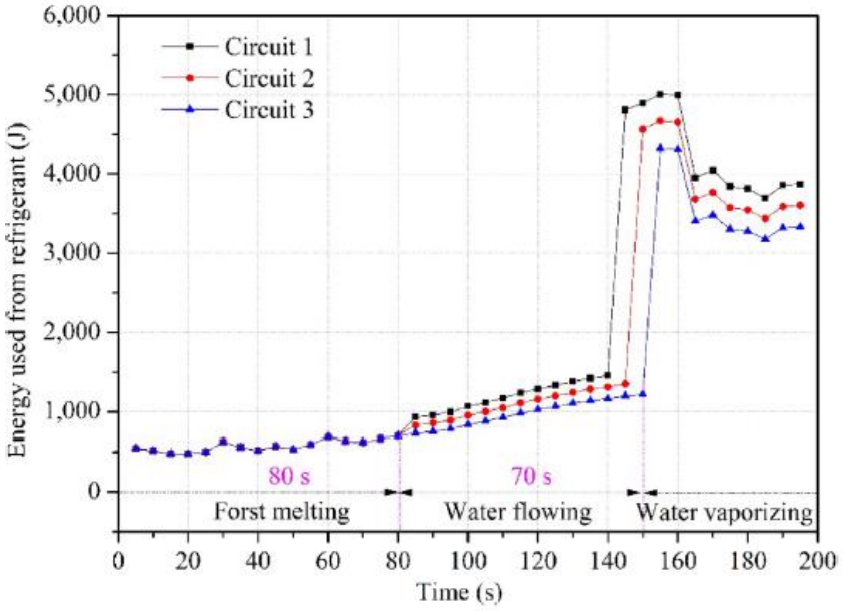

Fig. 13. Energy used from the refrigerant at each 5 s in Case 1.

The negative effects of the melted frost flowing show us at the Periods 2-5. In **Fig. 12**, the curves of three circuits also show us the 5 periods, just like that shown in **Fig. 11**. However, at the Period 1, similar to those shown in **Figs. 8 and 10**, the predicted results in Case 2 are not totally same to those in Case 1. This results from the inputs of two cases at the preheating stage are also different, as shown in **Figs. 3-6**. In addition, because the melted frost was locally drained, the heat transfer between refrigerant and the tube and fin was enhanced. Therefore, in most periods, the thermal resistance for three circuits are higher than those of Circuits 2 and 3 in Case 1, while a little lower than that of Circuit 1 in Case 1. The thermal resistance of refrigerant at Period 2 is at about 2.0 x 10^{-4} K*m^2/W, and reaches a peak at Period 4 at about 3.5 x 10^{-4} K*m^2/W in two cases.

Figs. 13 and 14 show the calculated energy used for defrosting from the refrigerant at each 5 s in Cases 1 and 2, respectively. They are calculated by the enthalpy difference between inlet and outlet of heat exchanger. The enthalpy values of refrigerant at inlet and outlet are calculated by using the temperature and pressure obtained. In **Fig. 13**, from 0 s to 80 s into defrosting, the energy is always lower than 1,000 J. At the water flowing stage, a period of 70 s after the frost melting stage, the energy used steadily increased to about 1,100 ~ 1,400 J for three circuits. Then, the suddenly increase point occur at 140 s, 145 s and 150 s for Circuit 1-3, with their peak value at about 5,000 J, 4,700 J and 4,400 J, respectively. This results from the vaporization of the melted frost, which is also reflected in the **Fig. 11**.

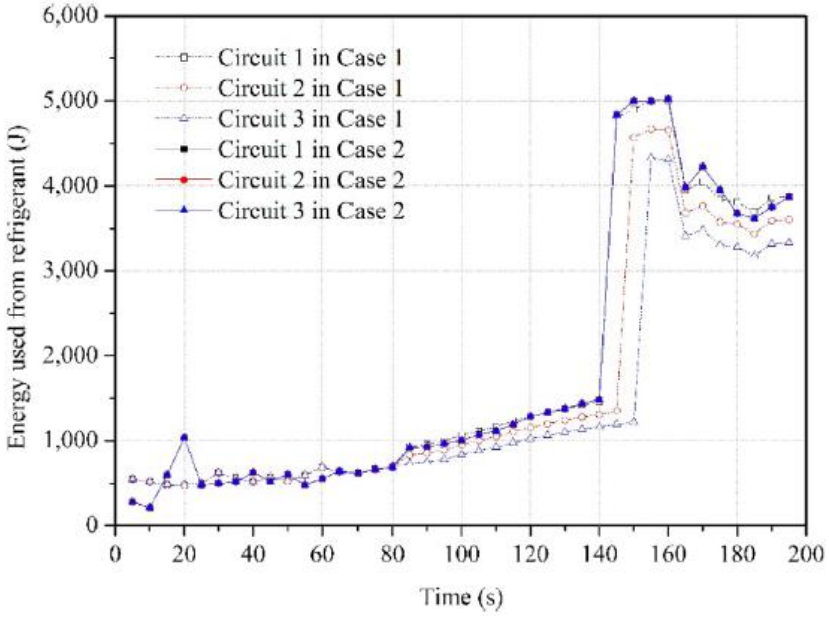

Fig. 14. Energy used from the refrigerant at each 5 s in Case 2.

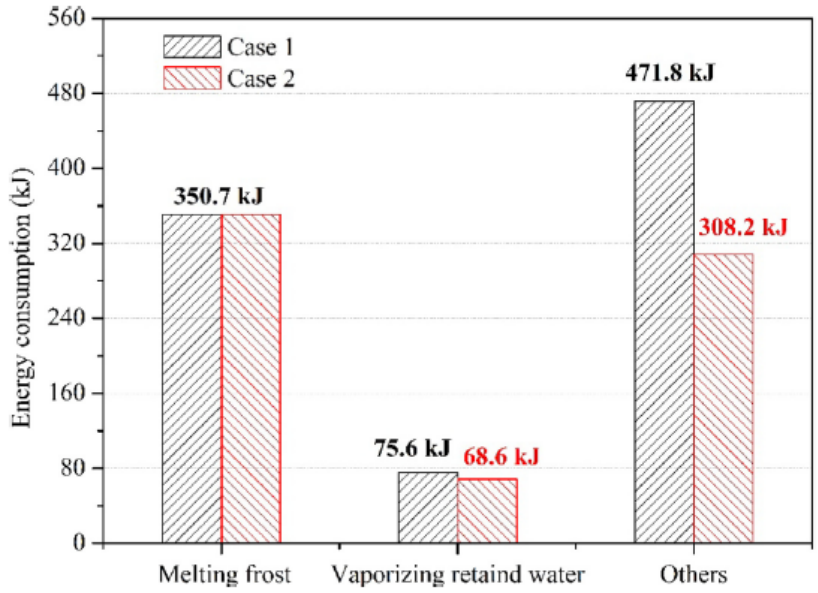

Fig. 15. Energy consumptions during defrosting in two cases.

The negative effects of melted frost downwards flowing also could be found in the water flowing and vaporizing stages in **Fig. 13**. **Fig. 14** show the energy used for defrosting from the refrigerant at each 5 s in Case 2. Compared with those curves shown in **Fig. 13**, curves of three circuits in Case 2 are always the same, and similar to the curve of Circuit 1 shown in Case 1.

It could also be concluded that, after the melted frost locally drained during defrosting, the energy consumption from refrigerant could be higher, which makes the defrosting process much quicker than that in Case 1.

During an ASHP unit operated at reverse cycle defrosting mode, the energy from refrigerant could be used for heating the tube and fin, melting the frost, heating the melted frost, heating the ambient air, vaporizing the melted and residual water, etc. To analyze the energy transfer process during defrosting, it is meaningful to predicted the aforementioned energy consumptions. As shown in Fig. 15, the energy consumptions in melting frost and vaporizing residual water are firstly predicted, at 350.7 kJ for two cases, and at 75.6 kJ and 68.6 kJ for Cases 1 and 2, respectively.

Table 2 Energy consumptions and the defrosting efficiency in the two cases

Item	Parameter	Case 1	Case 2
1	Heating melted frost (kJ)	7.2	2.0
2	Heating ambient air (kJ)	397.7	255.7
3	Heating metal and residual water (kJ)	66.9	50.5
4	Total energy from refrigerant (kJ)	898.1	727.5
5	Predicted defrosting efficiency	47.5%	57.6%
6	Experimental defrosting efficiency	43.5%	56.7%

At the same time, all the other energy consumption sections are summarized, at 471.8 kJ for Case 1 and 308.2 kJ for Case 2, respectively. Clearly, only the energy used for melting frost are nearly the same due to the same frost accumulations at the start of defrosting mode. All the other sections are different due to the melted frost was taken away in Case 2. The detailed of other energy consumptions are listed in Table 2. As seen, the heating melted frost, heating ambient air, heating metal of tube and fin and the residual water energy consumptions are 7.2 kJ and 2.0 kJ, 397.7 kJ and 255.7 kJ, 66.9 kJ and 50.5 kJ for Cases 1 and 2, respectively. Total energy used from refrigerant is calculated at 898.1 kJ and 727.5 kJ for two cases. It could be found that, at all items, the values in Case 1 are more than those in Case 2. The predicted defrosting efficiencies are 47.5% and 57.6 for Cases 1 and 2, respectively. And the experimental defrosting efficiency were calculated at 43.5% and 56.7% for two cases [**30**]. After the melted frost locally drained during defrosting, the efficiency was effectively improved. The errors of defrosting efficiencies in two cases are very small and acceptable, at 4% and 0.9%.

4. Discussions

In the model developed by Xu et al. [**39**], two different heat transfer regions, (1) a superheated region and (2) a two-phase region, existed in the refrigerant side of the outdoor coil. However, in this study, during the defrosting models developed, the entire outdoor coil was regarded as having a two-phase region only [**28,34**]. Heat exchanges between refrigerant and frost/ambient air in the sub-cooling

region and the superheated region in the outdoor coil were both neglected during defrosting. To analyze whether there is the sub-cooling and superheated region at the inlet and outlet of outdoor coil during reverse cycle defrosting, it was analyzed by using the experimental data from Case 1 reported in Ref. [**30**]. After the defrosting mode is operated about 50 s, the pressure values at the compressor discharge and EEV enter points and the temperatures at the inlet and outlet of outdoor coil are collected. As shown in **Fig. 16**, the two refrigerant status points at the inlet and outlet of outdoor coil are located at Points A and B, respectively. There is some pressure loss in the copper tube from the compressor discharge point to the inlet of outdoor coil and from outlet of outdoor coil to the inlet of EEV, the locations for A and B will be moved to left and right a little. But the status of refrigerant at Points A and B are at the sub-cooling and superheated regions, respectively. That means, the two regions exist during defrosting, and further development work should be directed to considering all three regions for an improved modeling accuracy.

As shown in **Fig. 17**, a defrosting process on the surface of outdoor coil could be divided into the following four stages when we want to analyze the effect of melted frost, (1) preheating, (2) frost melting without water flowing away from a circuit, (3) frost melting with water flowing away from a circuit, and (4) water layer vaporizing. But sometimes, the aforementioned Stages 2 and 3 could be summarized to melting stage. When we want to further analyze the residual water, the water layer vaporizing stage could be further divided into evaporating stage and dry-heating stage. This division method, with five stages, was also considered in the modeling of Qiao [**26**], as shown in **Fig. 17**(a). Clearly, the defrosting process is a complicated heat transfer and flow coupled problem. This is also the reason why the defrosting behavior and performance on vertical plate for surfaces of varying wettability were experimentally investigated by Kim et al. [**40**]. In this study, the model was developed with lumper method, and thus the defrosting process on a circuit or a fin could not be analyzed. During the frost melting stage, a thin water layer or film between a vertical hydrophobic fin surface and the frost will form, as shown in **Fig. 17**(b).

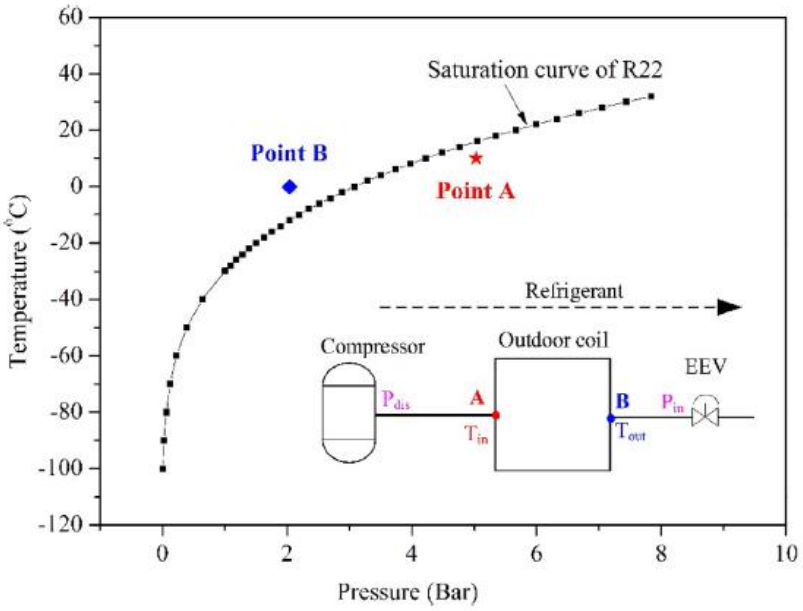

Fig. 16. Analysis of refrigerant status at the inlet and outlet of outdoor coil

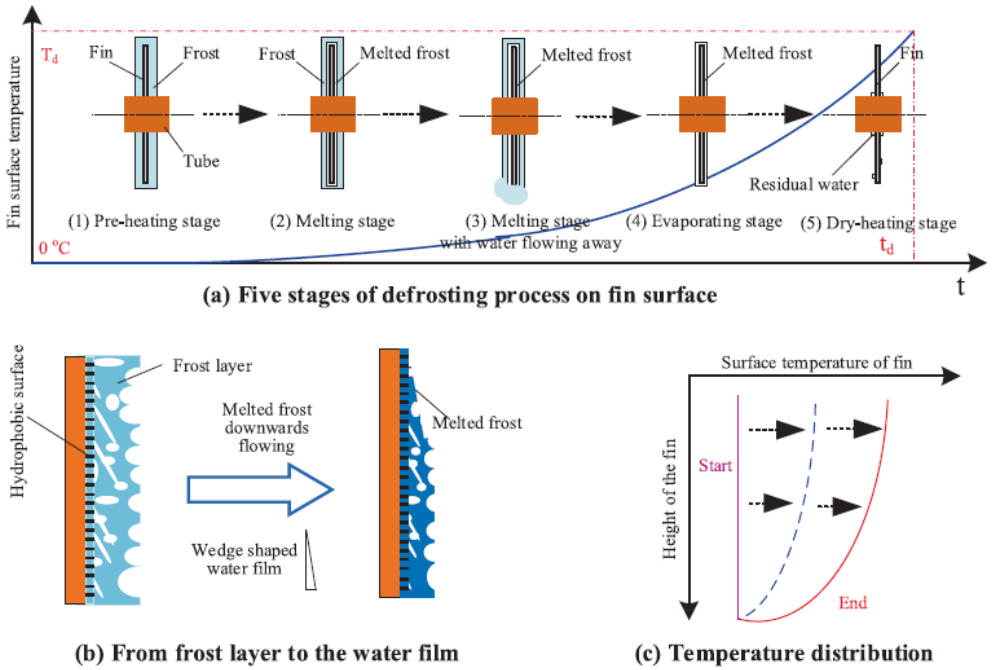

Fig. 17. Illustration of defrosting process on a vertical flat fin.

It will be a wedge-shaped water film, and the horizontal heat transfer between water layer and frost exists, as well as the infiltration and adsorption of water into the multi-porous frost layer due to the surface tension of water. As shown in **Fig. 17**(c), along the height of fin, the surface temperature of fin will be changed as the defrosting process. A smaller scale defrosting model will be developed in our future work.

5. Conclusions

A numerical investigation on the defrosting performance of an ASHP unit was carried out, with the melted frost downwards flowing away and local drainage considered. Basing on the previously developed and validated dynamic defrosting models, new inputs parameters, such as refrigerant temperatures, were used. Four typical parameters about defrosting were simulated and results analyzed, including the temperature of melted water on each circuit's surface, the mass of melted frost, thermal resistance of refrigerant, and energy consumptions during defrosting in two cases. As analyzed, the negative effects of melted frost could be reflected in all the four parameters when compared the predicted values in the case of melted frost downwards flowing away or two cases. The parameters of total thermal resistance of refrigerant are predicted at about 2.0 x 10^{-4} K^*m^2/W at the melted frost flowing stage, and 3.5 x 10^{-4} K^*m^2/W at the vaporizing water stage in two cases. The system defrosting efficiency was predicted, and compared with the experimental values. The deviations are very small, at 4% and 0.9% for two cases. The refrigerant status at the inlet and outlet of outdoor coil are analyzed, with the subcooling and superheated regions discussed. In our further development work, the two regions will be considered for an improved modeling accuracy. Meanwhile, a smaller scale defrosting mode for a circuit or a fin will be developed, to further analyze the heat transfer and water flow coupled effect during defrosting on the surface of a vertical fin. The contribution of this work are expected to be useful for intelligent control of ASHP units, as well as the energy saving in building and industry.

References

[1] Q.L Zhang, L Zhang, J.Z. Nie, Y.L Li, Techno-economic analysis of air source heat pump applied for space heating in northern China, Appl. Energy 207 (2017)533-542.

[2] Y.J. Fang, L.J. Chen, S.W. Mei, W. Wei, F. Liu, Coal or electricity? An evolutionary game approach to investigate fuel choices of urban heat supply systems, Energy. 181 (2019) 107-122.

[3] A. Pillarisetti, R.J. Ma, M. Buyan, B. Nanzad, K.R. Smith, Advanced household heat pumps for air pollution control: A pilot field study in Ulaanbaatar, the coldest capital city in the world, Environ. Res. 176 (2019) 108381.

[4] M.J. Song, S.M. Deng, C.B. Dang, N. Mao, Z.H. Wang, Review on improvement for air source heat pump units during frosting and defrosting, Appl. Energy 211 (2018) 1150-1170.

[5] D. Huang, Q.X. Li, X.L. Yuan, Comparison between hot-gas bypass defrosting and reverse-cycle defrosting methods on an air-to-water heat pump, Appl. Energy 86 (2009) 1697-1703.

[6] M. Amer, C.C. Wang, Review of defrosting methods, Renew. Sustain. Energy Rev. 73 (2017) 53-74.

[7] Y.J. Ding, G.Y. Ma, Q.H. Chai, Y. Jiang, Experiment investigation of reverse cycle defrosting methods on air source heat pump with TXV as the throttle regulator, Int. J. Refrig 27 (2004) 671-678.

[8] W.J. Hu, Y.Q. Jiang, M.L. Qu, L. Ni, S.M. Deng, An experimental study on the operating performance of a novel reverse-cycle hot gas defrosting method for air source heat pumps, Appl. Therm. Eng. 31 (2011) 363-369.

[9] M.L. Qu, Y.B. Tang, T.Y. Zhang, Z. Li, J.B. Chen, Experimental investigation on the multi-mode heat discharge process of a PCM heat exchanger during TES based reverse cycle defrosting using in cascade air source heat pumps, Appl. Therm. Eng. 151 (2019) 154-162.

[10] M.L. Qu, R. Zhang, J.B. Chen, Y.D. Cheng, Z. Li, Experimental analysis of heat coupling during TES based reverse cycle defrosting method for cascade air source heat pumps, Renewable Energy 147 (2020) 35-42.

[11] B.W. Yang, J.K. Dong, L. Zhang, M.J. Song, S.M. Deng, Heating and energy storage characteristics of multi-split air source heat pump based on energy storage defrosting, Appl. Energy 238 (2019) 303-310.

[12] J.K. Dong, S. Li, Y. Yao, Y.Q. Jiang, H. Tian, Defrosting performances of a multisplit air source heat pump with phase change thermal storage, Int. J. Refrig 55 (2015) 49-59.

[13] Z.B. Liu, F. Zhao, L.F. Zhang, R. Zhang, Y.Y. Chi, Performance of bypass cycle defrosting system using compressor casing thermal storage for air-cooled household refrigerators, Appl. Therm. Eng. 130 (2018) 1215-1223.

[14] Z.B. Liu, A. Li, Q.H. Wang, Y.Y. Chi, L.F. Zhang, Experimental study on a new type of thermal storage defrosting system for frost-free household refrigerators, Appl. Therm. Eng. 118 (2017) 256-265.

[15] M.J. Song, A.L. Chen, N. Mao, An experimental study on defrosting performance of an ASHP unit with a multi-circuit outdoor coil at different frosting evenness values, Appl. Therm. Eng. 94 (2016) 331-334.

[16] M.J. Song, N. Mao, S.M. Deng, Y.D. Xia, Y. Chen, An experimental study on defrosting performance for an air source heat pump unit at different frosting evenness values with melted frost locally drainage, Appl. Therm. Eng. 99 (2016) 730-740.

[17] W. Wang, J. Xiao, Y.C. Feng, Q.C. Guo, L.C. Wang, Characteristics of an ASHP with novel photoelectric sensors during periodic frost-defrost cycles, Appl. Therm. Eng. 50 (2013) 177-186.

[18] Y. Chung, S.I. Na, J.M. Choi, M.S. Kim, Feasibility and optimization of defrosting control method with differential pressure sensor for air source heat pump systems, Appl. Therm. Eng. 155 (2019) 461-469.

19] M.H. Kim, K.S. Lee, Determination method of defrosting start-time based on temperature measurements, Appl. Energy 146 (2015) 263-269.

[20] J.W. Yoo, Y. Chung, G.T. Kim, C.W. Song, M.S. Kim, Determination of defrosting start time in an air-to-air heat pump system by frost volume calculation method, Int. J. Refrig 96 (2018) 169-178.

[21] M.J. Song, Z.H. Wang, N. Mao, J.K. Dong, H.R. Zhang, Defrosting start control strategy optimization for an air source heat pump unit with the frost accumulation and melted frost downwards flowing considered, Sustainable Cities and Society. 46 (2019) 101461.

[22] M.J. Song, G.C. Gong, N. Mao, S.M. Deng, Z.H. Wang, Experimental investigation on an air source heat pump unit with a three-circuit outdoor coil for its reverse cycle defrosting termination temperature, Appl. Energy 204 (2017) 13881398.

[23] Z.Q. Liu, G.F. Tang, F.Y. Zhao, Dynamic simulation of air-source heat pump during hot-gas defrost, Appl. Therm. Eng. 23 (2003) 675-685.

[24] A.M. Alebrahim, S.A. Sherif, Electrical defrosting analysis of a finned tube evaporator coil using the enthalpy method, Proc Inst Mech Eng, Part C: J Mech Eng Sci 216 (2002) 655-673.

[25] W.J. Hu, M.J. Song, Y.Q. Jiang, Y. Yao, Y. Gao, A modeling study on the heat storage and release characteristics of a phase change material based doublespiral coiled heat exchanger in an air source heat pump for defrosting, Appl. Energy 236 (2019) 877-892.

[26] H.T. Qiao, K. Aute, R. Radermacher, Modeling of transient characteristics of an air source heat pump with vapor injection during reverse-cycle defrosting, Int. J. Refrig 8 (2018) 24-34.

[27] D.H. Niederer, Frosting and defrosting effects on coil heat transfer, ASHRAE Trans. 82 (1976) 467-473.

[28] M.L. Qu, D.M. Pan, L. Xia, S.M. Deng, Y.Q. Jiang, A study of the reverse cycle defrosting performance on a multi-circuit outdoor coil unit in an air source heat pump-Part II: Modeling analysis, Appl. Energy 91 (2012) 274-280.

[29] A.M. Rahman, A.M. Jacobi, Study of frost properties and frost melt water drainage on microgrooved brass surfaces in multiple frost/defrost/refrost cycles, Appl. Therm. Eng. 64 (2014) 453-461.

[30] M.J. Song, S.M. Deng, D.M. Pan, N. Mao, An experimental study on the effects of downwards flowing of melted frost over a vertical multi-circuit outdoor coil in an air source heat pump on defrosting performance during reverse cycle defrosting, Appl. Therm. Eng. 67 (2014) 258-265.

[31] M.J. Song, D.M. Pan, N. Li, S.M. Deng, An experimental study on the negative effects of downwards flow of the melted frost over a multi-circuit outdoor coil in an air source heat pump during reverse cycle defrosting, Appl. Energy 138 (2015) 598-604.

[32] M.J. Song, S.M. Deng, N. Mao, X.M. Ye, An experimental study on defrosting performance for an air source heat pump unit with a horizontally installed multi-circuit outdoor coil, Appl. Energy 165 (2016) 371-382.

[33] M.J. Song, C.B. Dang, N. Mao, S.M. Deng, Energy transfer procession in an air source heat pump unit during defrosting with melted frost locally drainage in its multi-circuit outdoor coil, Energy Build. 164 (2018) 109-120.

[34] M.J. Song, S.M. Deng, L Xia, A semi-empirical modeling study on the defrosting performance for an ASHP unit with local drainage of melted frost from its three-circuit outdoor coil, Appl Energy 136 (2014) 537-547.

[35] M.J. Song, L. Xia, S.M. Deng, A modeling study on alleviating uneven defrosting for a vertical three-circuit outdoor coil in an air source heat pump unit during reverse cycle defrosting, Appl. Energy 161 (2016) 268-278.

[36] C. Shen, J.F. Ma, J.H. Pu, Y.H. Hu, S.M. Deng, The effect of PM2.5 air pollution on the frosting process of outdoor finned-tube evaporator, Energy Build. 213 (2020) 109808.

[37] T.W. Lai, P. Ding, X. Dong, Y.u. Beile Zhang, Hou., Experimental study on the frosting characteristics of round tube in confined circular flow path at low temperature, Appl. Therm. Eng. 171 (2020) 115075.

[38] W. Wang, S.Q. Zhang, Z.Y. Li, Y.Y. Sun, X. Wu, Determination of the optimal defrosting initiating time point for an ASHP unit based on the minimum loss coefficient in the nominal output heating energy, Energy. 191 (2020) 116505.

[39] G.Y. Xu, X.S. Zhang, S.M. Deng, A simulation study on the operating performance of a solar-air source heat pump water heater, Appl. Therm. Eng. 26 (2006) 1257-1265.

[40] H. Kim, G.R. Jin, J.Y. Jeon, K.S. Lee, D.R. Kim, Defrosting behavior and performance on vertical plate for surfaces of varying wettability, Int. J. Heat Mass Transf. 1 (2018) 481-489.